Title
Multiple Decay Mechanisms and 2D-UV Spectroscopic Fingerprints of Singlet Excited Solvated Adenine-Uracil Monophosphate

Journal
Chemistry - A European Journal, 22(22)

ISSN
0947-6539

Authors
Li, Quansong
Giussani, Angelo
Segarra-Martí, Javier
et al.

Publication Date
2016-05-23

DOI
10.1002/chem.201505086

ChemPubSoc Europe

DOI: 10.1002/chem.201505086

CHEMISTRY A European Journal Full Paper

Photophysics |*Hot Paper*|

Multiple Decay Mechanisms and 2D-UV Spectroscopic Fingerprints of Singlet Excited Solvated Adenine-Uracil Monophosphate

Quansong Li,[d] Angelo Giussani[+],[b] Javier Segarra-Martí[+],[b] Artur Nenov,[b] Ivan Rivalta,[c] Alexander A. Voityuk,[a, e] Shaul Mukamel,[f] Daniel Roca-Sanjuán,[g] Marco Garavelli,*[b, c] and Lluís Blancafort*[a]

Abstract: The decay channels of singlet excited adenine uracil monophosphate (ApU) in water are studied with CASPT2//CASSCF:MM potential energy calculations and simulation of the 2D-UV spectroscopic fingerprints with the aim of elucidating the role of the different electronic states of the stacked conformer in the excited state dynamics. The adenine ^1L_a state can decay without a barrier to a conical intersection with the ground state. In contrast, the adenine ^1L_b and uracil S(U) states have minima that are separated from the intersections by sizeable barriers. Depending on the backbone conformation, the CT state can undergo inter-base hydrogen transfer and decay to the ground state through a conical intersection, or it can yield a long-lived minimum stabilized by a hydrogen bond between the two ribose rings. This suggests that the ^1L_b, S(U) and CT states of the stacked conformer may all contribute to the experimental lifetimes of 18 and 240 ps. We have also simulated the time evolution of the 2D-UV spectra and provide the specific fingerprint of each species in a recommended probe window between 25000 and 38000 cm^{-1} in which decongested, clearly distinguishable spectra can be obtained. This is expected to allow the mechanistic scenarios to be discerned in the near future with the help of the corresponding experiments. Our results reveal the complexity of the photophysics of the relatively small ApU system, and the potential of 2D-UV spectroscopy to disentangle the photophysics of multichromophoric systems.

Introduction

The photophysics of DNA and its components is a paramount example of synergy between experiment and theory.[1] A large number of time-resolved spectroscopic experiments and ab initio computations have been conducted to study the interaction between UV light and DNA, making the nucleobases a benchmark for the development of time-resolved pump-probe spectroscopy. As a result, the fundamental photophysical properties of the isolated canonical nucleobases are well understood today. Ultrashort excited-state lifetimes arise because of highly efficient radiationless mechanisms that are considered to offer self-protection against UV damage. The challenge now is to understand more complex systems, including DNA itself, which present notably different photophysics compared with the isolated nucleobases. Their decay mechanisms

[a] *Prof. A. A. Voityuk, Prof. L. Blancafort*
Institut de Química Computacional i Catàlisi and Departament de Química
Universitat de Girona, Campus de Montilvi, 17071 Girona (Spain)
E-mail: lluis.blancafort@udg.edu

[b] *Dr. A. Giussani,[+] Dr. J. Segarra-Martí,[+] Dr. A. Nenov, Prof. M. Garavelli*
Dipartimento di Chimica "G. Ciamician", Università di Bologna
Via Selmi 2, 40126 Bologna (Italy)
E-mail: marco.garavelli@unibo.it

[c] *Dr. I. Rivalta, Prof. M. Garavelli*
Univ Lyon, Ens de Lyon, CNRS, Université Lyon 1
Laboratoire de Chimie UMR 5182, 69342, Lyon (France)

[d] *Dr. Q. Li*
Key Laboratory of Cluster Science of Ministry of Education
School of Chemistry, Beijing Institute of Technology
100081 Beijing (P.R. China)

[e] *Prof. A. A. Voityuk*
Institució Catalana de Recerca i Estudis Avançats (ICREA)
08010 Barcelona (Spain)

[f] *Prof. S. Mukamel*
Department of Chemistry, University of California, Irvine
California 92697-2025 (USA)

[g] *Dr. D. Roca-Sanjuán*
Instituto de Ciencia Molecular, Universitat de València
P. O. Box 22085, 46071 Valencia (Spain)

[+] *These authors contributed equally to this work.*

Supporting information for this article is available on the WWW under http://dx.doi.org/10.1002/chem.201505086.

are controversial, and different types of states (locally excited states, delocalized states such as excimers, exciplexes or excitons, or charge transfer (CT) states) have been proposed to be important.

To clarify the mechanistic picture, new spectroscopic developments are expected to play a crucial role. Among them, bidimensional UV (2D-UV) spectroscopy[2] appears particularly promising because it can be used to overcome the intrinsic low spectral resolution of one-dimensional spectroscopy, allowing the disentanglement of the overlapping bands found in a one-dimensional spectrum. Consequently, it gives the possibility of selectively tracking the de-excitation pathways that correspond to different transitions activated with a broadband pump pulse, opening the way for a more detailed mechanistic interpretation of the photoinduced processes experienced by a system. 2D-UV spectroscopy has already been applied experimentally to the study of the photophysics of the nucleobases[3] as well as in light-harvesting complexes.[4]

In the present contribution, we focus on the photophysics of the adenine uracil diribonucleoside monophosphate (ApU, see Scheme 1) in water. Dinucleosides are an ideal test ground to understand the relevant excited-state species in more complex systems because, due to their relatively small size, they can be modeled at a high level of theory. ApU in solution has a complex photodynamics with three components of 2.0 ± 0.1, 18 ± 6, and 240 ± 70 ps measured with transient absorption spectroscopy after 267 nm excitation.[5] The results have been explained in terms of two groups of stacked and unstacked conformers. The decay components of 2.0 and 240 ps, which are also seen for a mixture of the adenine and uracil ribonucleoside monophosphates, are assigned to the unstacked conformers. They correspond, respectively, to the monomer-like decay of the individual nucleobases, and a long-lived channel of the uracil ribonucleoside that may correspond to an ($n\pi^*$) or triplet state.[6] The 18 ps component was assigned to an adenine→uracil CT state, because the results for a set of five dinucleotides show an inverse relationship between the lifetime of this component and the energy of the CT state estimated from the ionization potentials and electron affinities of the two bases involved in it.[5] The appearance of the CT component was also postulated in a study on the closely related dApT molecule, using picosecond time-resolved infrared spectroscopy for detection, for which the measured lifetime was 75 ps.[7]

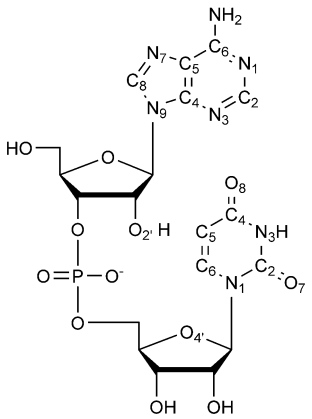

Scheme 1. ApU structure and atom labeling for adenine and uracil.

In this context, the main goal of our work is to elucidate the mechanism of the photophysics of ApU with the help of high-level potential energy calculations and simulation of the 2D-UV spectra. Our CASPT2//CASSCF:AMBER computations provide a global mechanistic picture that considers all relevant states. We find a complex photophysics in which both locally excited adenine and uracil states and the adenine→uracil CT state may contribute to the experimental 18 and 240 ps components. Such a complex picture calls for 2D-UV experiments that may disentangle the contributions of the different states to the spectrum, and therefore we have computed the characteristic 2D-UV spectral fingerprints of the computed relaxation pathways. These calculations provide the guidelines for future 2D-UV experiments that are expected to resolve the interpretation of the photophysics of ApU.

The signals decaying on the picosecond timescale, which are one of the main points of interest of our work, are a general feature of oligonucleotide molecules. Signals from 2.7 to longer than 200 ps have been described with different techniques for systems going from diribonucleoside monophosphates to single- and double-stranded oligomers.[5,8] However, the origin of the picosecond signals observed in these systems still constitutes an unsolved question. To date, four main explanations have been proposed. The first candidate is CT excimer or exciplex formation between two nucleobases. These species have been characterized in calculations on adenine- and thymine-based complexes,[9] and calculations on a pair of stacked adenines embedded in DNA for which they are proposed to arise from interconversion from the bright adenine ^1L_a state.[10] The involvement of CT states has also been postulated by assigning specific infrared transient absorption bands to these states.[7,8m,o,11] The second possibility is that the picosecond-range signals come from neutral excimers. This species has been characterized computationally for adenine dimers[12] and pyrimidine homodimers,[13] where it has been proposed as a precursor of the cyclobutane pyrimidine dimers. The third possibility is long-lived excitons delocalized over more than two bases.[14] Finally, the fourth candidate is excited states localized on the monomers, the lifetime of which compared with the gas phase is slowed down by environment. Calculations show that in adenine, the decay of the ^1L_a state is barrierless in the gas phase.[15] However, when the base is embedded in oligomers, barriers of 0.1–0.4 eV appear,[10,16] and the decay is slowed down in molecular dynamics compared with that in the gas phase.[17] In this context, the insight provided by our study of the photophysics of ApU will be relevant for other complex systems in which the same states appear as discussed here.

Results

Our computational system is ApU surrounded by a water sphere of 727 molecules, including a Na^+ counterion. Adenine and uracil are treated quantum mechanically (QM), and the

rest of the system is treated with molecular mechanics (MM) using ONIOM[18] and the AMBER force field. This hybrid approach is similar to those used in previous studies of nucleobase dinucleotides in solution or dimers embedded in oligomers.[10,12d,19] The potential energy study follows the CASPT2//CASSCF approach, which is well suited for excited states, for which the optimizations are carried out with CASSCF as the QM method, and the final energy is obtained with CASPT2. The final values are referred to as CASPT2:AMBER. The 2D-UV spectra are obtained with CASPT2 (see Computational Details at the end of this article and in the Supporting Information).

In solution, ApU is present in stacked and unstacked conformations. We assume that the time for interconversion between the stacked and unstacked forms exceeds the excited-state lifetimes, because the different forms have clearly distinguishable NMR signals.[20] In addition, the unstacked conformations are assumed to have very similar photophysics to the single nucleotides.[5] Based on these assumptions, we consider only the stacked conformer throughout our study. We also focus on the states involving the π-orbitals of the bases, because the oxygen and nitrogen lone pairs are expected to play a minor role due to their increased energy in water.

Absorption spectrum of stacked ApU

As a first step to understand the photodynamics of ApU, we calculated the absorption spectrum of the stacked conformer in water. To sample the accessible conformational space, the spectrum was calculated for ten snapshots extracted from a 1 ns ground-state molecular dynamics simulation, replacing the MM geometries of the bases by their idealized geometries[21] (details in Section SI1.2). The results, which are summarized as a plot in Figure 1, show the states at energies up to 5.6 eV (see detailed values in Table SI1). Below this threshold, one expects four states: the two lowest $\pi\pi^*$ states of adenine, of ^1L_a and ^1L_b character, the lowest uracil $\pi\pi^*$ state, S(U), and the CT state. The results agree with this picture. In most cases,

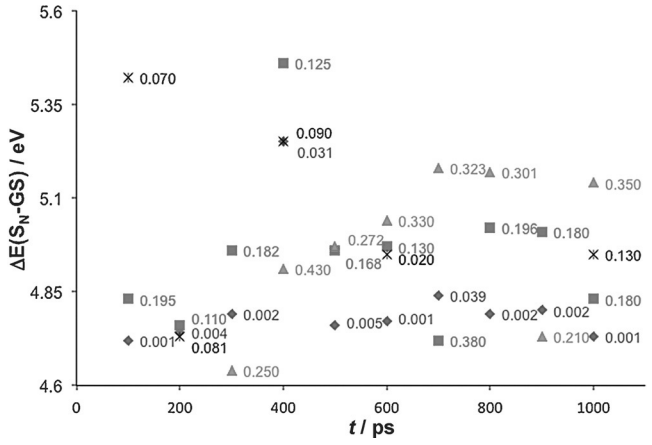

Figure 1. CASPT2:AMBER ApU vertical excitation energies and oscillator strengths at ten snapshots selected every 100 ps along a 1 ns ground-state molecular dynamics run; diamonds: A*pU-1L_b; squares: A*pU-1L_a; triangles: ApU*; asterisks: A^+pU^- state.

there is a weakly absorbing state, A*pU-^1L_b, and two strongly absorbing states, A*pU-^1L_a and ApU*. The identification of the ApU* state is not always straightforward, because a strong coupling leads to considerable mixing of the wave functions at some geometries, and this has prevented the assignment of the uracil localized transition at the 100 and 200 ps snapshots.

The average calculated excitations are 4.82 and 4.95 eV for the ^1L_b and ^1L_a states, respectively, and 4.97 eV for the S(U) state. If stacking effects on the absorption are ignored, these values are in satisfactory agreement with the absorption maxima in water of 4.77 eV for adenosine[22] (attributed to the ^1L_a state) and 4.73 eV for uridine monophosphate.[23] They are also comparable with previous CASPT2/MM based estimates of the vertical absorption in water, which are 4.99 and 5.01 eV for the ^1L_b and ^1L_a states,[24] respectively, and 4.99 eV for the S(U) state.[25] For the CT state, the average value is 5.51, and the A^+pU^- excitation energy is below 5.6 eV in five out of ten snapshots. Significantly, in three cases (snapshots at 200, 600 and 1000 ps) it has non-negligible oscillator strength and falls within 0.3 eV of the experimental excitation energy (4.64 eV or 267 nm).[5] This suggests that in a part of the conformational space the A^+pU^- state can be populated directly after excitation at 267 nm (4.64 eV).

The A^+pU^- vertical excitation energy varies greatly at the different snapshots. This is consistent with previous calculations on stacked AT pairs in water, which showed that the energy of the CT state is sensitive to the conformation, leading to a broad band, the red tail of which overlaps with the $\pi\pi^*$ states.[9c] One of the structural parameters that stabilizes the CT state is an intramolecular hydrogen bond in the nucleotide backbone formed between the hydrogen atom of the adenosine O2′-H group and the O4′ uridine atom (see atom numbering in Scheme 1 and distances in Table SI1). This intramolecular hydrogen bond stabilizes the A^+pU^- state by bringing together the charged bases, inducing a favorable electrostatic interaction. As we discuss below, this feature is also found for one of the CT state minima, $(A^+pU^-)_{min-2}$.

Potential-energy-surface characterization

To assign the experimental decay time constants, we have optimized the ground- and excited-state minima and the decay paths to the ground state. We consider two groups of structures to account for the flexibility of ApU, starting from the lowest energy conformation of the molecular dynamics run and a conformation with a low CT energy (600 ps in Figure 1). In both cases, the ground-state was reoptimized at the ONIOM(CASSCF:AMBER) level to obtain equilibrated structural parameters for the QM and MM parts. This leads to reference structures FC-1 and FC-2 (see Figure 2). The optimizations were carried out for both snapshots, yielding two sets of structures that differ in the conformation of the ribose rings and the mutual orientation of the bases. In the first group of structures the two bases are approximately parallel, and in the second group they have a more pronounced tilt with respect to each other (see Figure 2; details in Section SI1.3 and Table SI2). FC-1 is favored at the CASPT2:AMBER level by about 2.5 eV, but

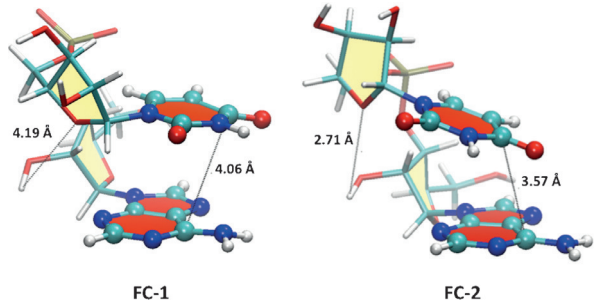

Figure 2. CASSCF:AMBER ground-state-optimized structures including representative distances in Å. In the present and following images, the rings are colored by pucker, using the Cremer–Pople pucker amplitude, as implemented in VMD.[26]

this value is not representative of the relative stability in solution because it comes from potential energy minimization and not from dynamics.

For both groups of structures, relaxation of the ^1L_b, S(U) and CT states leads to minima for these states, whereas optimization of the ^1L_a state leads to a conical intersection with the ground state. For the first group of structures we have also optimized a doubly excited minimum, $(ApU)^*_{min-1}$, for which the dominant excited state configuration has four unpaired electrons in the frontier molecular orbitals of the adenine and uracil fragments, but this state was not considered further because of its high relative energy (6.35 eV). The A*pU-^1L_b and ApU* minima display monomer-localized distortions on the excited nucleobase similar to those found for the isolated monomers, whereas the structure of the complementary base is unchanged. The minima found for the first group of structures are displayed in Figure 3, whereas those found for the second group of structures are displayed in the Supporting Information together with the bond lengths (see Figure SI1, SI2).

The locally excited minima can decay to the ground state through conical intersection structures analogous to those reported for the monomers, characterized by an out-of-plane bending of the adenine C2–H[15] and the uracil C5–H[15i,27] group, respectively. The out-of-plane bending can take place with the hydrogen atom pointing towards the complementary base or in the opposite direction, which leads to *endo* and *exo* conical intersection isomers, respectively. We have located the two isomers for the adenine- and uracil-centered intersections in both sets of structures, and estimated the barriers to access the conical intersections with constrained optimizations along linear interpolation paths (see Section SI1.4 for details). The most energetically favorable intersections for the first group of structures are displayed in Figure 3. The remaining structures are provided in the Supporting Information, together with the energy profiles along the decay paths (Figures SI1–SI7). For the uracil-centered minima $(ApU^*)_{min-1}$ and $(ApU^*)_{min-2}$, the lowest barriers to reach the $(ApU^*/gs)_{CI}$ intersections are 0.17 and 0.23 eV, respectively (see Table 1). For the adenine-centered structures $(A^*pU\text{-}^1L_b)_{min-1}$ and $(A^*pU\text{-}^1L_b)_{min-2}$, the decay involves a switch to the ^1L_a state, and the lowest barriers to reach the $(A^*pU\text{-}^1L_a/gs)_{CI}$ intersections are 0.68 and 0.59 eV.

Turning to the CT state, the minima obtained for the two groups of structures present notable differences. $(A^+pU^-)_{min-1}$ has a strong, stabilizing hydrogen bond (1.82 Å) between the O8 carbonyl oxygen atom of the negatively charged uracil and one of the amino hydrogen atoms of the positively charged adenine. From this structure there is an almost barrierless path

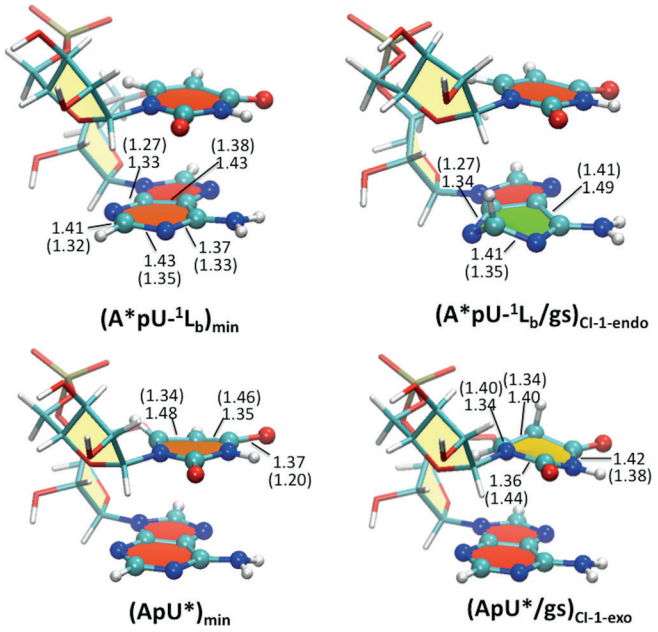

Figure 3. CASSCF:AMBER optimized critical points for the monomer-localized excited states, using FC-1 as reference geometry. Representative bond lengths are given in Å (ground-state values in parentheses).

Table 1. Relative CASPT2:AMBER energies (eV) of the characterized critical points with respect to the FC-1 (group 1) and FC-2 (group 2) ground-state energy. Vertical emission energies are reported for the different minima in round brackets, and barriers from the minima to the conical intersections in square brackets.

Structure	Group 1 E_{rel} [eV]	Group 2 E_{rel} [eV]
FC[a]	0.00	0.00[b]
	4.70 (^1L_b)	4.92 (^1L_b)
	4.88 (^1L_a)	5.07 (^1L_a)
	5.42, 5.49[c]	5.39 (S(U))
	6.01 (CT)	5.77 (CT)
$(A^*pU\text{-}^1L_b)_{min}$[d]	4.56 (4.51)	4.46 (4.40)
$(ApU^*)_{min}$[d]	5.42 (3.69)	4.70 (3.77)
$(A^+pU^-)_{min}$[d]	3.02 (2.51)	4.19 (2.14)
$(ApU)^*_{min}$[d]	6.35 (4.46)	–
$(A^*pU\text{-}^1L_a/gs)_{CI-exo}$[e]	4.30 [0.75]	3.96 [0.59]
$(A^*pU\text{-}^1L_a/gs)_{CI-endo}$[e]	4.14 [0.68]	4.45 [0.79]
$(ApU^*/gs)_{CI-exo}$[f]	4.30 [0.17]	3.82 [0.33]
$(ApU^*/gs)_{CI-endo}$[f]	4.78 [0.24]	3.89 [0.23]
$(A^+pU^-/gs)_{CI}$[g]	2.37 [<0.1]	–

[a] Vertical excitation spectrum, state assignment in brackets. [b] Relative energy of FC-2 with respect to FC-1: 2.49 eV. [c] Mixed states which cannot be assigned unequivocally. [d] Vertical emission energy in brackets. [e] Barrier to access the intersection from $(A^*pU\text{-}^1L_b)_{min}$ in square brackets. [f] Barrier to access the intersection from $(ApU^*)_{min}$ in square brackets. [g] Barrier to access the intersection from $(A^+pU^-)_{min-1}$ in square brackets.

(< 0.1 eV) for hydrogen transfer from the adenine to the uracil fragment (see the Supporting Information, Figure SI4), similar to interstrand excited state hydrogen transfer in AT pairs.[28] This leads to a conical intersection mediated by electron and hydrogen transfer, $(A^+pU^-/gs)_{Cl-1}$, which is similar to those described for other biomolecule pairs.[29] $(A^+pU^-/gs)_{Cl-1}$ provides an efficient deactivation channel to the ground state, followed by reversion of the hydrogen transfer. This suggests that $(A^+pU^-)_{min-1}$ may not be the species responsible for the long-lived experimental signal.

In contrast to $(A^+pU^-)_{min-1}$, the minimum found for the second group of structures, $(A^+pU^-)_{min-2}$, is stabilized by a hydrogen bond between the O2′-H group of the adenosine ribose and the O4′ atom of the ribose group of uridine (1.85 Å), and an electrostatic interaction between the negatively charged uracil O8 atom and the positively charged adenine C6 atom (see Figure 4). The hydrogen transfer path is not favored and $(A^+pU^-)_{min-2}$ may be a long-lived species, because we could not find any low-energy conical intersection that could facilitate its decay to the ground state.

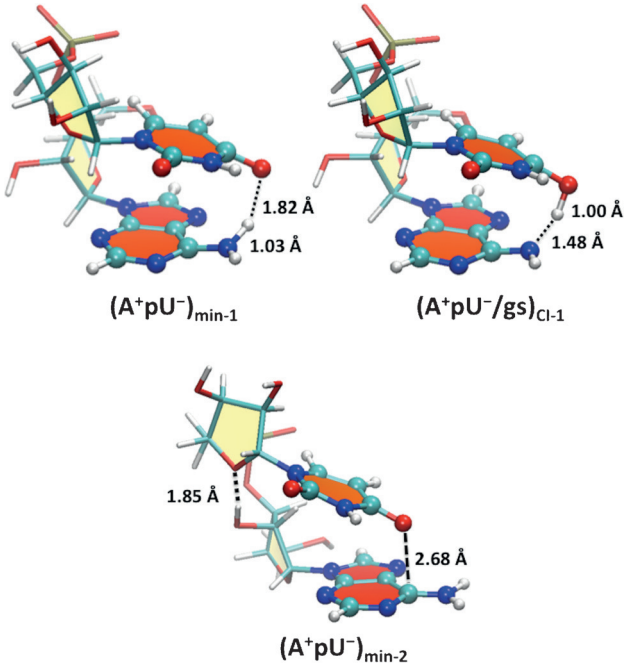

Figure 4. CASSCF:AMBER optimized minima for the CT A^+pU^- state, using FC-1 and FC-2 as reference geometries, and conical intersection associated to $(A^+pU^-)_{min-1}$. Representative bond lengths are given in Å.

To summarize the potential energy surface calculations, excitation at 267 nm can populate several excited states that show different behavior. The ^1L_a state of adenine has no stable minimum and can decay to the ground state without a barrier, whereas the weakly absorbing ^1L_b state and the uracil-localized S(U) state have stable minima that are separated from the conical intersections that facilitate the radiationless decay by barriers of approximately 0.6 and 0.2 eV, respectively. For comparison, barrierless decay paths for the S(U) state of unsubstituted uracil[30] and thymine[31] in water have been found by using similar approaches. This suggests that the lifetime of the S(U) state in ApU will exceed that measured for thymine, uracil or their nucleosides in water, which is approximately 2 ps.[5,8g] Similarly, the lifetime of the ^1L_b state in ApU will exceed that measured for adenine or its nucleoside. Presumably, the barriers encountered in ApU to access the base-centered intersections arise because the bases are distorted and favorable interactions between the stacked bases are disrupted. This seems to be a general effect, because it is found for all conformations of these intersections.

Finally, the lifetime of the CT state depends greatly on the conformation of the ribose rings. In the second group of structures with ${}^4_3T$ and ${}^2_1T$ conformation in the adenosine and uridine sugars, respectively, there is a stable minimum that will contribute to the longer-lived excited-state components. The vertical emission energy of $(A^+pU^-)_{min-2}$ is 2.14 eV (579 nm). This is consistent with the emission of 2.7 eV associated with a decay component with 72 ps lifetime measured in the alternating $d(AT)_{10}$ oligomer, which was assigned to a stacked AT excimer with A→T CT character.[8h]

In this complex scenario, the simulated 2D-UV spectra presented in the following section provide specific fingerprints for the different states and yield valuable information about how to assess experimentally which are the actual molecular motions that promote the long-lived channels.

2D-UV simulation

Recent experiments[32] and theoretical simulations[33] have demonstrated that 2D-IR can be employed to recognize structural motifs (tertiary structure) in peptides. It is anticipated that 2D-UV can be as valuable for resolving base stacking through its weak, but detectable, effects on the positions and intensities of the electronic transitions of the bases.[34] A high accuracy of the electronic structure and a calibration of the methods is essential to capture these effects.[35]

The aim of the present study is to differentiate spectroscopically the electronic excited-state decay pathways. We center on the main characteristic features of each electronic state, that is, its local stimulated emission (SE) and bright excited-state absorption (ESA) signals that qualify as candidates for experimental detection. They are less sensitive to the base stacking but exhibit pronounced spectral shifts of several thousands of cm^{-1} during the excited-state relaxation dynamics, which allows a qualitative discussion that is less dependent on the computational accuracy, and we will show that the current simulations are in good agreement with benchmark studies carried out on isolated adenine[36] and uracil.[37]

Our 2D-UV simulation is based on the specific fingerprints of the minima associated with the different states involved in the photodynamics. Our main assumption is that population gets trapped along the relaxation pathway in local minima and the barrier to access the conical intersection gives rise to the lifetime of the excited state. Consequently, the electronic structure of the minima will dominate the time-resolved spectrum for pump-probe delays in the order of the excited-state lifetime.

The spectral traces of the ^1L_b, S(U) and CT states have been calculated for the two groups of structures presented in the previous section. Both sets gave similar results; therefore, we only discuss the results for the second group. The spectra for the first group are presented in the Supporting Information (Figure SI8–SI10). For simplicity, only the key signals for the experimental characterization are discussed. Schematic diagrams are also provided (see Figure 5 c,f,i) in which ground-state bleach (GSB) (solid line) and SE (dashed line) transitions are drawn in blue and ESAs in red. The same color code is used in the spectra. The gray color used in some of the diagrams denotes signals that fall outside the probing window of 25 000–44 000 cm^{-1}. The spectral traces of the ^1L_a state are not presented in Figure 5 because this state is expected to have a very short life time, which will result in a broad, unstructured trace dominated by ESA.

We start by discussing the trace of the ^1L_b state. The spectrum in the FC region (see Figure 5 a) shows two prominent transient absorption signals. The first, labeled 3, is placed at approximately 34 000 cm^{-1} along Ω_3 and arises from a transition from the ^1L_b state to an adenine centered doubly excited state (D_1*(A)). This is in agreement with our recent state-of-the-art computations,[36] which demonstrate that the range between 20 000 and 36 000 cm^{-1} is dominated by the ESA to the D_1*(A) state. The second signal (peak 5) lies in the high-energy window at approximately 42 000 cm^{-1} and corresponds to additional excitation of an adenine to uracil CT state (^1L_b + CT). As the initially populated ^1L_b state evolves towards its minimum (A*pU-^1L_b)$_{min-2}$ (cf. Figure 5 b), its energy relative to the FC region shifts to the red. This yields a characteristic emission feature 1′ that appears in a shifted region of the spectrum and provides, together with a slight redshift in signal 3, unique fingerprints that can be used to identify this structure.

We turn our attention next to the uracil S(U) state and the evolution of its high-lying excited state manifold. Figure 5 d,e show the spectra of the FC-2 and (ApU*)$_{min-2}$ geometries correlated with the S(U) transition of uracil (ca. 42 000 cm^{-1}). A schematic representation of the different electronic transitions is given for visual aid on the right of Figure 5 f. The gray color denotes signals that fall outside the probing window due to large shifts. Peaks 1 and 2 arise from GSB of the ^1L_b and ^1L_a states of adenine, and peaks 3 and 3′ come from GSB and SE of the S(U) state, which have the same energy at the FC region. At this region (see Figure 5 d), the S(U) manifold shows only two ESA contributions, peaks 4 and 5, which correspond to a double excitation on uracil, D_1*(U), and a simultaneous S(U) + ^1L_a excitation, respectively. This is consistent with high accuracy computations for the FC region of uracil for which only a few characteristic ESA signals (transitions to doubly excited states) are found between 34 000 and 20 000 cm^{-1}.[37] The intense peak 5 in the high-energy window at approximately 37 000 cm^{-1} lies just above the GSB peak 2 and provides direct evidence for noncovalent interactions. These weak interactions cause the emergence of GSB/ESA pairs (2 and 5 in this case) with a signal splitting proportional to the coupling strength. After relaxation, a very pronounced shift in the signals can be readily noted in the spectrum at (ApU*)$_{min-2}$ (see Figure 5 e).

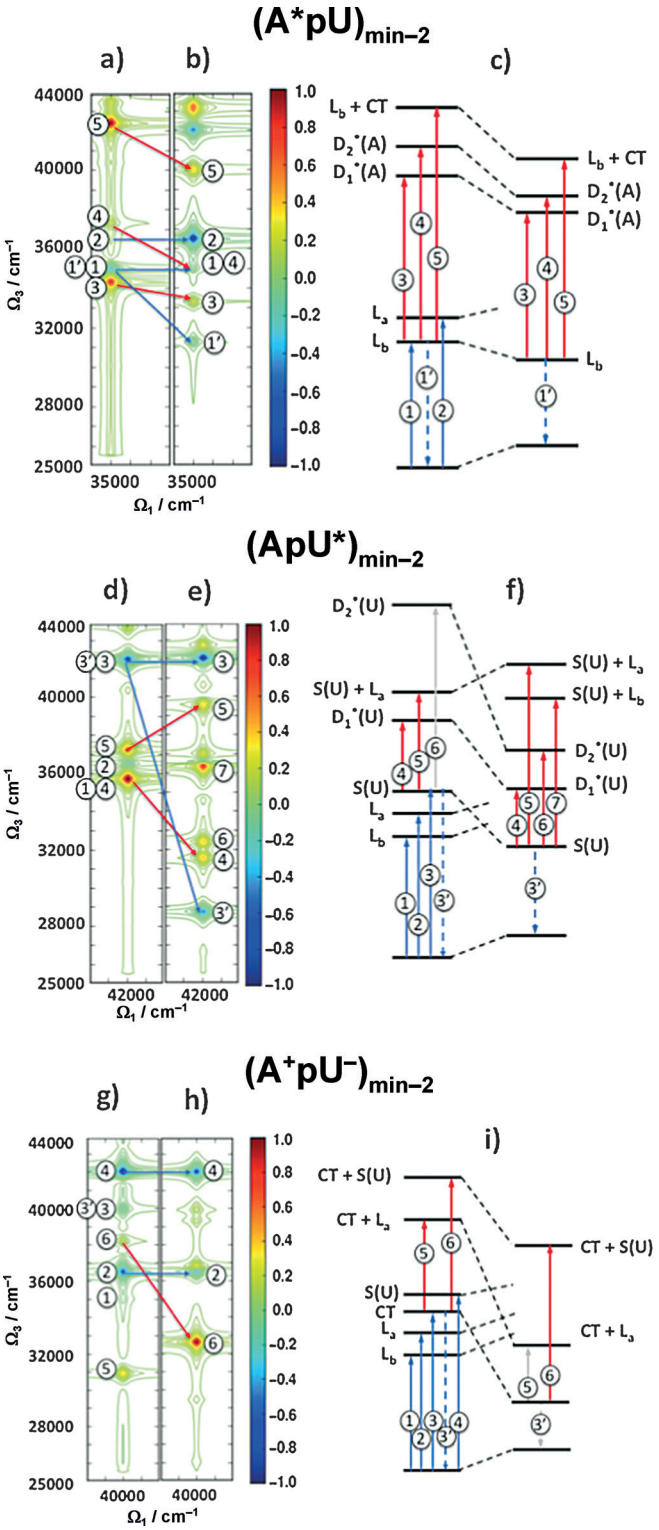

Figure 5. 2D NUV-pump NUV-probe spectra (NUV: near UV) for the different traces analyzed in the present study: ^1L_b manifold at a) FC-2 and b) (A*pU-^1L_b)$_{min-2}$, and c) energy-level diagram describing the different transitions along the ^1L_b trace; S(U) manifold at d) FC-2 and e) (ApU*)$_{min-2}$, and f) energy-level diagram describing the transitions along the S(U) trace; CT manifold at g) FC-2 and h) (A^+pU^-)$_{min-2}$, and i) energy-level diagram depicting the transitions along the CT trace. The energy labels along the *x* axis (Ω_1) correspond to the energy of the main trace, and the small ticks along the axes indicate 1000 cm^{-1} shifts.

The SE signal undergoes a large redshift of approximately 13000 cm^{-1}. This strong stabilization, which is related to the pronounced geometrical rearrangements suffered by the uracil moiety, also shifts peaks 4 and 6 strongly to the red and places them at approximately 32000 cm^{-1}. Given the characteristics of the analyzed spectra, peaks 3′, 4, and 6 appear to be in energetic regions that provide the best fingerprint to register the ApU* state spectroscopically.

The last state to be considered is the CT state. The spectra of the FC-2 and $(A^+pU^-)_{min-2}$ geometries are shown in Figure 5g,h. At the FC region (see Figure 5g), the CT manifold shows several GSB signals related to the ^1L_b, ^1L_a, CT and S(U) states, yielding peaks 1–4, respectively. In this case, the CT features non-negligible oscillator strength associated with its transition. Two ESA signals corresponding to excitation to CT + ^1L_a and CT + S(U) states can be discerned. These peaks, 5 and 6, are situated at approximately 31000 and 38000 cm^{-1} along Ω_3, respectively. After relaxation, $(A^+pU^-)_{min-2}$ (see Figure 5h) shows pronounced shifts in both ESA and SE signals (peaks 3, 5, and 6) due to the large nuclear rearrangements. Peak 6 suffers a strong redshift of approximately 6000 cm^{-1} down to approximately 33000 cm^{-1}, which is a relatively empty energy window in which the contributions from $(A^+pU^-)_{min-2}$ might be probed experimentally, given the strong intensity of this signal. In turn, peaks 3′ and 5 appear below the 25000 cm^{-1} mark after relaxation. Although they lie outside our present probing window, they would be the best fingerprints for lower-energy probe experiments.

Discussion

The proposed time evolution of the 2D-UV spectra for the stacked ApU conformer is presented in Figure 6. Based on our potential energy calculations, we propose three main steps: early times, dominated by barrierless decay of the ^1L_a state (left panel), intermediate times before the decay of the S(U) state (middle panel), and late times after the decay of this state (right panel). In the early events of the photodynamics, within the femtosecond timescale (left side of the spectrum in Figure 6), the spectrum is governed by intense contributions from the ^1L_a and S(U) manifolds, which cover the rest of the signals. Along the ^1L_a trace, we present the signals from the FC region, which include a singly excited adenine state, S(A), characterized by a H-1→L+1 transition, a doubly excited state D* (H→L transition), a negative signal in the diagonal composed of SE and GSB, and a high-lying, combined ^1L_a + S(U) ESA. This ESA, paired with the near-lying bleach signal at Ω_1 = 36500 cm^{-1}, Ω_3 = 42000 cm^{-1}, is indicative of the noncovalent interaction between the two bases. However, because of the ultrafast relaxation and the ultrashort lifetime of the ^1L_a state, and based on our benchmarking studies,[36] we expect that these peaks will merge into a broad, unstructured signal already at sub-100 fs waiting times, covering also the much weaker ^1L_b trace. Along the S(U) trace, one finds the equivalent bleach/ESA pair at Ω_1 = 42000 cm^{-1}, Ω_3 = 36500 cm^{-1} (signals 5 and 2 in Figure 5d), and the doubly excited D_1*(U) state (signal 4 in Figure 5d).

Moving to the picosecond timescale, the contributions arising from the ^1L_a state vanish as its population depletes, leaving the contributions from the relaxed ^1L_b, CT and S(U) channels, which decay at longer times. At this stage of the dynamics (middle spectrum in Figure 6), the S(U) state gathers most of the intensity and covers the rest of the states. The spectrum features the main fingerprints characterizing $(ApU^*)_{min-2}$, ascribed to doubly excited ESAs (D_1* and D_2*, peaks 4 and 6 in Figure 5e) and its SE (peak 3′ in Figure 5e), with a barely noticeable contribution from the CT state (CT + S(U), peak 6 in Figure 5h). At longer times (right side spectrum in Figure 6), the bright contributions from the S(U) manifold are expected to vanish based on the computed barriers, giving way to the contributions from the CT and ^1L_b states to be registered. The trace associated with the CT state is expected to be significantly broadened because of the dependence of its absorption energy and oscillator strength on the conformational dynamics. Therefore, the CT + S(U) signal along this trace (corresponding to peak 6 in Figure 5h) may be considerably lower in intensity than what is shown in Figure 6 right panel. Another characteristic signature of the CT trace should be the absence of signals in the red, except for the ESA to the CT + ^{1}La state at 24000 and the SE at 20000 cm^{-1} (transitions 5 and 3′ in Figure 5i). The ^1L_b state can be expected to provide a small contribution because it will be populated mainly in an indirect way during the decay of the ^1L_a state.[15d,f] However, it should still be possible to monitor it in the spectra because it displays characteristic ^1L_b(SE) emission (peak 1′ in Figure 5b), which is also visible for bare adenine,[36] and ^1L_b + CT signals around its trace along Ω_1 (peak 5 in Figure 5b) in a region that is otherwise relatively free of signals.

Overall, the theoretical spectra strongly suggest that it would be beneficial to shift the probe window to the low-energy region of the UV, where identifiable fingerprints in the form of SE and ESAs emerge.[36] The near-UV is very suitable to track excited-state dynamics because it is background-free, that is, there are no contributions from solute or solvent photoionization or fragmentation, which allows for high signal-to-noise ratios even with weak probe intensities. This spectral window also depends less on the level of theory employed for the simulation, thus endorsing the reliability of the predicted spectra.[36] Broadband probe pulses will be essential to capture the predicted shifts of more than 10000 cm^{-1} and track the complete photophysics process. Self-phase modulation with a supercontinuum source seems capable of achieving this goal,[38] thus encouraging new experimental setups that will be feasible soon with the present technological advances and can provide unequivocal insight into the state-specific dynamics of DNA/RNA dimeric and oligomeric systems.

Conclusion

The main aim of the present study is to provide qualitatively new insight into the photophysics of a nucleobase dimer, ApU, with state-of-the-art computational chemistry. We have centered on the stacked conformer that is suggested to be responsible for the appearance of an 18 ps signal in the experi-

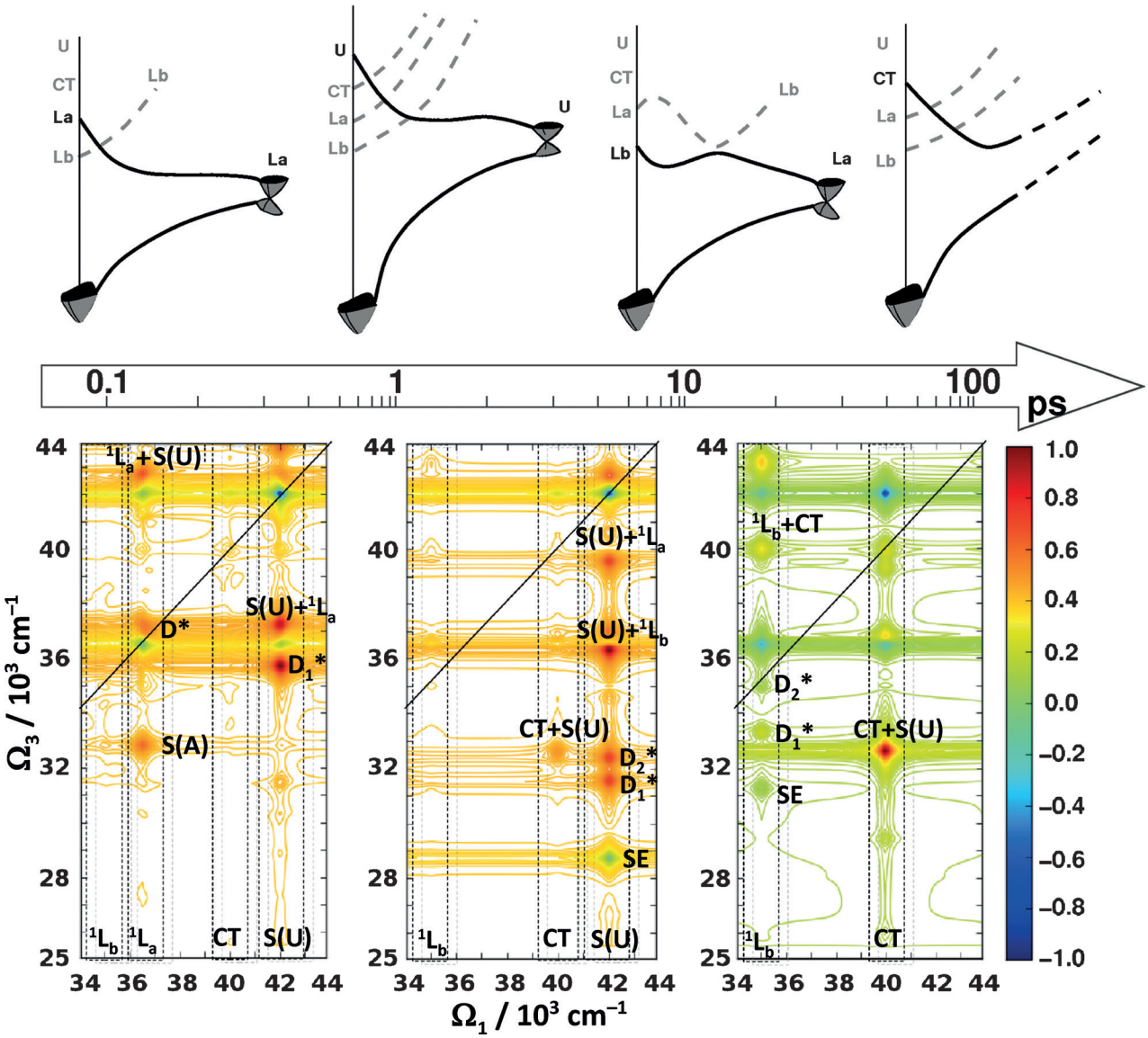

Figure 6. Proposed time evolution of the 2D NUV-pump NUV-probe spectra for stacked ApU. The time arrow marks approximately the scale at which the spectra will evolve according to the potential energy calculations. Left panel: early times; middle panel: intermediate times; right panel: late times. A schematic description of the relaxation channels of each state is provided at the top of the figure.

ments, and we have combined a detailed exploration of the excited-state potential energy surface at the CASPT2//CASSCF:AMBER level with the simulation of the 2D-UV electronic spectra using the SOS approach. The results show an unexpected complexity for a relatively simple system, formed by only two bases. In contrast to what is computed for the single nucleobases or nucleotides in water, the excited states localized on the single nucleobases have sizeable barriers to reach the conical intersections that induce the radiationless decay. This probably happens because favorable stacking interactions are disrupted when the nucleobases are distorted to reach the intersections, which results in energy barriers. In addition, the fate of the A→U CT state depends on the conformation of the ribose rings. These results can be reconciled with the original interpretation of the experiments,[5] which make the CT state responsible for the 18 ps component, if one assumes that the uracil S(U) state decays in the scale of a few picoseconds, regardless of the calculated barrier. However, an alternative mechanism is also possible whereby the uracil S(U) state is responsible for the measured 18 ps component and the contributions of the CT state (and eventually the adenine ^1L_b one) overlap with those of the long-lived uracil π,π* or triplet state of the unstacked conformers to give the 240 ps component measured in the transient absorption spectra.

The proposed mechanistic alternatives cannot be differentiated unambiguously by one-dimensional pump-probe spectroscopic approaches, for which the contributions of the different decay channels are superimposed. This task cannot be achieved by theoretical state-of-the-art non-adiabatic dynamics approaches either, because the underlying electronic structure methods are not accurate enough to treat the competition between the different paths correctly (see for instance the discus-

sions in ref. [39]). It is precisely in this context that the simulation of the 2D-UV electronic spectra becomes important, since it provides a specific fingerprint for every species, and this will make it possible to track the evolution of the different states experimentally in the near future. Our simulations show the most favorable spectral window in which this can be done. Therefore, the present study shows the potential of 2D-UV spectroscopy, combined with high-level computations, to provide new insights into the photophysics of nucleobase dimers and, by extension, other multichromophoric systems.

Experimental Section

Computational details

The potential energy surface calculations were carried out with a quantum mechanics/molecular mechanics (QM/MM) approach using the "Own N-layer Integrated molecular Orbital molecular Mechanics" (ONIOM)[18] method as implemented in Gaussian[40] and the complete active space self consistent field (CASSCF) level of theory. The excited-state minima and conical intersections were optimized at the ONIOM(CASSCF/6-31+G*:AMBER) level, treating the adenine and uracil bases quantum mechanically and the rest of the system with AMBER. To account for dynamic correlation, the energy of the structures was corrected calculating the state-specific complete active space second-order perturbation (SS-CASPT2) energy of the A-U model system with Molcas,[41] using the atomic natural orbital S-type (ANO-S) basis set[42] and including the MM charges in the calculation. The resulting values are referred to as CASPT2:AMBER. We used a link-atom scheme and electronic embedding with the charge equilibration approach.[43] During the optimizations, only the ApU molecule, the Na^+ ion and a solvation shell formed by the 84 closest molecules were allowed to relax, and the rest of the system was kept frozen. For a balanced treatment of the two bases in the optimization of the excited-state minima, we used an active space of four orbitals on each base, i.e., eight electrons in eight orbitals, denoted as (8,8). However, for the conical intersection optimizations, we used a different active space composed of all the π-orbitals from the base that carries the excitation ((12,10) and (10,8) for adenine and uracil, respectively) to give a better account of correlation energy at the CASSCF level and avoid large degeneracy-lifting effects with CASPT2. With this approach, we obtained small CASPT2 energy gaps at the intersections of $\leq$0.25 eV (see the Supporting Information, Figure SI3–SI7). For the CASPT2 potential energy calculations, we used a (12,12) active space (six orbitals from each base) to warrant a balanced treatment of all structures. More computational details are given in Section SI1.1.

Quasi-absorptive bidimensional electronic spectra were computed with a development version of Spectron 2.7.[44] For the spectra, energies were computed with the state-average SA-80-CASSCF(8,8)/SS-CASPT2/ANO-S protocol. These energies and the CASSCF transition dipole moments were coupled with the sum-over-states (SOS) technique[45] to compute the nonlinear response of the system.[46] The solvent was represented with the MM point charges. The pump pulses in Figure 5 were always positioned at the frequency of the electronic transition at the FC point, while probing a broad spectral region between 25000 and 44000 cm^{-1}. We used infinitely broad pulses for our simulations. This makes our simulations independent of the experimental setup and gives a qualitatively correct position of the peaks compared with the finite pulses that will be employed experimentally. The position of the CT manifold in the spectra is shifted from its calculated position of 49000 cm^{-1} to 40000 cm^{-1}, which is the energy window at which this state appears in the 600 ps snapshot of the molecular dynamics that defines the FC-2 region (see Figure 1). To compute the temporal evolution of the fingerprints of each de-excitation channel, we used a simplified protocol that does not require excited-state dynamics simulations. It works within the framework of the static approximation[47] and relies on the assumption that the spectral signatures of the intermediates dominate the spectrum at longer times if the system is trapped (and equilibrated) in the minima on a timescale much longer than the duration of the experiment (details in Section SI2.1).[48]

Acknowledgements

We acknowledge the participation of the late Luis Serrano-Andrés in the first stage of this work. L.B. and A.V. acknowledge financial support from the Spanish Ministry of Economy (CTQ2011-26573, CTQ2015-69363-P) and the Generalitat de Catalunya (2014SGR-1202) and the use of computer time at the Consorci de Serveis Universitaris de Catalunya. Q.L. acknowledges the National Natural Science Foundation of China (21303007). M.G. acknowledges support by the European Research Council Advanced Grant STRATUS (ERC-2011-AdG No. 291198) and the Agence Nationale de la Recherche for the 2015 project FEMTO-2DNA (Spectroscopie 2DUV: un nouvel outil pour l'étude de biomolécules, ANR-15-CE29-0010). D.R.-S. acknowledges support from the Generalitat Valenciana (GV2015-057) and the Spanish Ministry of Economy (project CTQ2014-58624-P and grant JCI-2012-13431). S.M gratefully acknowledges the support of the Chemical Sciences, Geosciences, and Biosciences division, office of Basic Energy Sciences, U.S. Department of Energy, and the National Science Foundation (grant CHE-1361516).

Keywords: ab initio calculations · DNA · molecular electronics · photophysics · UV/Vis spectroscopy

[1] a) C. E. Crespo-Hernández, B. Cohen, P. M. Hare, B. Kohler, *Chem. Rev.* **2004**, *104*, 1977–2019; b) *Radiation Induced Molecular Phenomena in Nucleic Acids: A Comprehensive Theoretical and Experimental Analysis* (Eds.: M. Shukla, J. Leszczynski): *Challenges and Advances in Computational Chemistry and Physics*, Vol. 5, Springer, Dordrecht (The Netherlands), **2008**; c) C. T. Middleton, K. de La Harpe, C. Su, Y. K. Law, C. E. Crespo-Hernández, B. Kohler, *Annu. Rev. Phys. Chem.* **2009**, *60*, 217–239; d) K. Kleinermanns, D. Nachtigallova, M. S. de Vries, *Int. Rev. Phys. Chem.* **2013**, *32*, 308–342; e) *Photoinduced Phenomena in Nucleic Acids I: Nucleobases in the Gas Phase and in Solvents* (Eds.: M. Barbatti, A. C. Borin, S. Ullrich), *Top. Curr. Chem.* Vol. 355, **2015**; f) *Photoinduced Phenomena in Nucleic Acids II: DNA Fragments and Phenomenological Aspects* (Eds.: M. Barbatti, A. C. Borin, S. Ullrich, *Top. Curr. Chem. Vol. 356*, **2015**; g) R. Improta, F. Santoro, L. Blancafort, *Chem. Rev.* **2016**, *116*, 3540–3593.

[2] a) C.-H. Tseng, S. Matsika, T. C. Weinacht, *Opt. Express* **2009**, *17*, 18788–18793; b) U. Selig, C.-F. Schleussner, M. Foerster, F. Langhojer, P. Nuernberger, T. Brixner, *Opt. Lett.* **2010**, *35*, 4178–4180.

[3] a) B. A. West, J. M. Womick, A. M. Moran, *J. Phys. Chem. A* **2011**, *115*, 8630–8637; b) C.-H. Tseng, P. Sandor, M. Kotur, T. C. Weinacht, S. Matsika, *J. Phys. Chem. A* **2012**, *116*, 2654–2661.

[4] a) D. Zigmantas, E. L. Read, T. Mancal, T. Brixner, A. T. Gardiner, R. J. Cogdell, G. R. Fleming, *Proc. Natl. Acad. Sci. USA* **2006**, *103*, 12672–12677; b) N. S. Ginsberg, J. A. Davis, M. Ballottari, Y.-C. Cheng, R. Bassi, G. R. Fleming, *Proc. Natl. Acad. Sci. USA* **2011**, *108*, 3848–3853.

[5] T. Takaya, C. Su, K. de La Harpe, C. E. Crespo-Hernández, B. Kohler, *Proc. Natl. Acad. Sci. USA* **2008**, *105*, 10285 – 10290.
[6] P. M. Hare, C. E. Crespo-Hernández, B. Kohler, *Proc. Natl. Acad. Sci. USA* **2007**, *104*, 435 – 440.
[7] G. W. Doorley, M. Wojdyla, G. W. Watson, M. Towrie, A. W. Parker, J. M. Kelly, S. J. Quinn, *J. Phys. Chem. Lett.* **2013**, *4*, 2739 – 2744.
[8] a) C. E. Crespo-Hernández, B. Cohen, B. Kohler, *Nature* **2005**, *436*, 1141 – 1144; b) W.-M. Kwok, C. Ma, D. L. Phillips, *J. Am. Chem. Soc.* **2006**, *128*, 11894 – 11905; c) D. Markovitsi, F. Talbot, T. Gustavsson, D. Onidas, E. Lazzarotto, S. Marguet, *Nature* **2006**, *441*, E7 – E7; d) D. Markovitsi, T. Gustavsson, F. Talbot, *Photochem. Photobiol. Sci.* **2007**, *6*, 717 – 724; e) D. Onidas, T. Gustavsson, E. Lazzarotto, D. Markovitsi, *Phys. Chem. Chem. Phys.* **2007**, *9*, 5143 – 5148; f) D. Onidas, T. Gustavsson, E. Lazzarotto, D. Markovitsi, *J. Phys. Chem. B* **2007**, *111*, 9644 – 9650; g) K. de La Harpe, C. E. Crespo-Hernández, B. Kohler, *ChemPhysChem* **2009**, *10*, 1421 – 1425; h) W.-M. Kwok, C. Ma, D. L. Phillips, *J. Phys. Chem. B* **2009**, *113*, 11527 – 11534; i) I. Vayá, F.-A. Miannay, T. Gustavsson, D. Markovitsi, *ChemPhysChem* **2010**, *11*, 987 – 989; j) K. de La Harpe, B. Kohler, *J. Phys. Chem. Lett.* **2011**, *2*, 133 – 138; k) C. Su, C. T. Middleton, B. Kohler, *J. Phys. Chem. B* **2012**, *116*, 10266 – 10274; l) J. Chen, A. K. Thazhathveetil, F. D. Lewis, B. Kohler, *J. Am. Chem. Soc.* **2013**, *135*, 10290 – 10293; m) D. B. Bucher, B. M. Pilles, T. Carell, W. Zinth, *Proc. Natl. Acad. Sci. USA* **2014**, *111*, 4369 – 4374; n) J. Chen, B. Kohler, *J. Am. Chem. Soc.* **2014**, *136*, 6362 – 6372; o) B. M. Pilles, D. B. Bucher, L. Liu, P. Gilch, W. Zinth, W. J. Schreier, *Chem. Commun.* **2014**, *50*, 15623 – 15626.
[9] a) F. Santoro, V. Barone, R. Improta, *Proc. Natl. Acad. Sci. USA* **2007**, *104*, 9931 – 9936; b) F. Santoro, V. Barone, R. Improta, *ChemPhysChem* **2008**, *9*, 2531 – 2537; c) A. W. Lange, J. M. Herbert, *J. Am. Chem. Soc.* **2009**, *131*, 3913 – 3922; d) F. Santoro, V. Barone, R. Improta, *J. Am. Chem. Soc.* **2009**, *131*, 15232 – 15245; e) H. Yin, Y. Ma, J. Mu, C. Liu, M. Rohlfing, *Phys. Rev. Lett.* **2014**, *112*, 228301.
[10] I. Conti, A. Nenov, S. Hoefinger, S. F. Altavilla, I. Rivalta, E. Dumont, G. Orlandi, M. Garavelli, *Phys. Chem. Chem. Phys.* **2015**, *17*, 7291 – 7302.
[11] Y. Y. Zhang, J. Dood, A. A. Beckstead, X. B. Li, K. V. Nguyen, C. J. Burrows, R. Improta, B. Kohler, *Proc. Natl. Acad. Sci. USA Proc. Nat. Acad. Sci. USA* **2014**, *111*, 11612 – 11617.
[12] a) G. Olaso-González, M. Merchán, L. Serrano-Andrés, *J. Am. Chem. Soc.* **2009**, *131*, 4368 – 4377; b) R. Improta, V. Barone, *Angew. Chem. Int. Ed.* **2011**, *50*, 12016 – 12019; *Angew. Chem.* **2011**, *123*, 12222 – 12225; c) A. Banyasz, T. Gustavsson, D. Onidas, P. Changenet-Barret, D. Markovitsi, R. Improta, *Chem. Eur. J.* **2013**, *19*, 3762 – 3774; d) F. Plasser, H. Lischka, *Photochem. Photobiol. Sci.* **2013**, *12*, 1440 – 1452.
[13] a) D. Roca-Sanjuán, G. Olaso-González, I. González-Ramírez, L. Serrano-Andrés, M. Merchán, *J. Am. Chem. Soc.* **2008**, *130*, 10768 – 10779; b) I. González-Ramírez, D. Roca-Sanjuán, T. Climent, J. J. Serrano-Pérez, M. Merchán, L. Serrano-Andrés, *Theor. Chem. Acc.* **2011**, *128*, 705 – 711.
[14] I. Buchvarov, Q. Wang, M. Raytchev, A. Trifonov, T. Fiebig, *Proc. Natl. Acad. Sci. USA* **2007**, *104*, 4794 – 4797.
[15] a) H. Chen, S. H. Li, *J. Phys. Chem. A* **2005**, *109*, 8443 – 8446; b) C. M. Marian, *J. Chem. Phys.* **2005**, *122*, 104314; c) S. Perun, A. L. Sobolewski, W. Domcke, *J. Am. Chem. Soc.* **2005**, *127*, 6257 – 6265; d) L. Blancafort, *J. Am. Chem. Soc.* **2006**, *128*, 210 – 219; e) L. Serrano-Andrés, M. Merchán, A. C. Borin, *Proc. Natl. Acad. Sci. USA* **2006**, *103*, 8691 – 8696; f) L. Serrano-Andrés, M. Merchán, A. C. Borin, *Chem. Eur. J.* **2006**, *12*, 6559 – 6571; g) M. Barbatti, H. Lischka, *J. Am. Chem. Soc.* **2008**, *130*, 6831 – 6839; h) I. Conti, M. Garavelli, G. Orlandi, *J. Am. Chem. Soc.* **2009**, *131*, 16108 – 16118; i) A. Giussani, J. Segarra-Martí, D. Roca-Sanjuán, M. Merchán, in *Photoinduced Phenomena in Nucleic Acids I: Nucleobases in the Gas Phase and in Solvents, Vol. 355* (Eds.: M. Barbatti, A. C. Borin, S. Ullrich), Springer, Heidelberg/Berlin (Germany), **2015**, pp. 57 – 97.
[16] a) I. Conti, P. Altoe, M. Stenta, M. Garavelli, G. Orlandi, *Phys. Chem. Chem. Phys.* **2010**, *12*, 5016 – 5023; b) X. Chen, W. Fang, H. Wang, *Phys. Chem. Chem. Phys.* **2014**, *16*, 4210 – 4219.
[17] Y. Lu, Z. Lan, W. Thiel, *Angew. Chem. Int. Ed.* **2011**, *50*, 6864 – 6867; *Angew. Chem.* **2011**, *123*, 6996 – 6999.
[18] M. Svensson, S. Humbel, R. D. J. Froese, T. Matsubara, S. Sieber, K. Morokuma, *J. Phys. Chem.* **1996**, *100*, 19357 – 19363.
[19] a) V. A. Spata, S. Matsika, *J. Phys. Chem. A* **2013**, *117*, 8718 – 8728; b) V. A. Spata, S. Matsika, *Phys. Chem. Chem. Phys.* **2015**, *17*, 31073 – 31083.
[20] F. S. Ezra, C. H. Lee, N. S. Kondo, S. S. Danyluk, R. H. Sarma, *Biochemistry* **1977**, *16*, 1977 – 1987.
[21] L. Clowney, S. C. Jain, A. R. Srinivasan, J. Westbrook, W. K. Olson, H. M. Berman, *J. Am. Chem. Soc.* **1996**, *118*, 509 – 518.
[22] W. Voelter, R. Records, E. Bunnenbe, C. Djerassi, *J. Am. Chem. Soc.* **1968**, *90*, 6163 – 6170.
[23] J. M. Ploeser, H. S. Loring, *J. Biol. Chem.* **1949**, *178*, 431 – 437.
[24] V. Ludwig, Z. M. da Costa, M. S. do Amaral, A. C. Borin, S. Canuto, L. Serrano-Andrés, *Chem. Phys. Lett.* **2010**, *492*, 164 – 169.
[25] C. Bistafa, H. C. Georg, S. Canuto, *Comput. Theor. Chem.* **2014**, *1040*, 312 – 320.
[26] W. Humphrey, A. Dalke, K. Schulten, *J. Mol. Graphics Modell.* **1996**, *14*, 33 – 38.
[27] a) S. Matsika, *J. Phys. Chem. A* **2004**, *108*, 7584 – 7590; b) M. Z. Zgierski, S. Patchkovskii, T. Fujiwara, E. C. Lim, *J. Phys. Chem. A* **2005**, *109*, 9384 – 9387; c) M. Merchán, R. González-Luque, T. Climent, L. Serrano-Andres, E. Rodríguez, M. Reguero, D. Peláez, *J. Phys. Chem. B* **2006**, *110*, 26471 – 26476; d) H. R. Hudock, B. G. Levine, A. L. Thompson, H. Satzger, D. Townsend, N. Gador, S. Ullrich, A. Stolow, T. J. Martínez, *J. Phys. Chem. A* **2007**, *111*, 8500 – 8508.
[28] a) J. P. Gobbo, V. Saurí, D. Roca-Sanjuán, L. Serrano-Andrés, M. Merchán, A. C. Borin, *J. Phys. Chem. B* **2012**, *116*, 4089 – 4097; b) Y. Zhang, K. de La Harpe, A. A. Beckstead, R. Improta, B. Kohler, *J. Am. Chem. Soc.* **2015**, *137*, 7059 – 7062.
[29] a) L. Blancafort, J. Bertran, M. Sodupe, *J. Am. Chem. Soc.* **2004**, *126*, 12770 – 12771; b) A. L. Sobolewski, W. Domcke, *Phys. Chem. Chem. Phys.* **2004**, *6*, 2763 – 2771; c) L. Serrano-Andrés, M. Merchán, *Chem. Phys. Lett.* **2006**, *418*, 569 – 575.
[30] Y. Mercier, F. Santoro, M. Reguero, R. Improta, *J. Phys. Chem. B* **2008**, *112*, 10769 – 10772.
[31] A. Nakayama, G. Arai, S. Yamazaki, T. Taketsugu, *J. Chem. Phys.* **2013**, *139*, 214304 – 214304.
[32] B. Guchhait, Y. Liu, T. Siebert, T. Elsaesser, *Struct. Dyn.* **2016**, *3*, 043202.
[33] Z. Lai, N. K. Preketes, S. Mukamel, J. Wang, *J. Phys. Chem. B* **2013**, *117*, 4661 – 4669.
[34] a) A. Nenov, I. Rivalta, G. Cerullo, S. Mukamel, M. Garavelli, *J. Phys. Chem. Lett.* **2014**, *5*, 767 – 771; b) A. Nenov, S. A. Beccara, I. Rivalta, G. Cerullo, S. Mukamel, M. Garavelli, *ChemPhysChem* **2014**, *15*, 3282 – 3290.
[35] A. Nenov, S. Mukamel, M. Garavelli, I. Rivalta, *J. Chem. Theory Comput.* **2015**, *11*, 3755 – 3771.
[36] A. Nenov, A. Giussani, J. Segarra-Marti, V. K. Jaiswal, I. Rivalta, G. Cerullo, S. Mukamel, M. Garavelli, *J. Chem. Phys.* **2015**, *142*, 212443.
[37] A. Giussani, J. Segarra-Marti, A. Nenov, I. Rivalta, A. Tolomelli, S. Mukamel, M. Garavelli, *Theor. Chem. Acc.* **2016**, *135*, 121.
[38] N. Krebs, I. Pugliesi, J. Hauer, E. Riedle, *New J. Phys.* **2013**, *16*, 085016.
[39] a) L. Blancafort, *Photochem. Photobiol.* **2007**, *83*, 603 – 610; b) D. Asturiol, B. Lasorne, M. A. Robb, L. Blancafort, *J. Phys. Chem. A* **2009**, *113*, 10211 – 10218; c) M. Barbatti, Z. Lan, R. Crespo-Otero, J. J. Szymczak, H. Lischka, W. Thiel, *J. Chem. Phys.* **2012**, *137*, 22A503; d) F. Plasser, R. Crespo-Otero, M. Pederzoli, J. Pittner, H. Lischka, M. Barbatti, *J. Chem. Theory Comput.* **2014**, *10*, 1395 – 1405; e) L. Blancafort, *ChemPhysChem* **2014**, *15*, 3166 – 3181; f) J. Segarra-Martí, M. Garavelli, F. Aquilante, *J. Chem. Theory Comput.* **2015**, *11*, 3772 – 3784.
[40] M. J. Frisch, G. W. Trucks, H. B. Schlegel, G. E. Scuseria, M. A. Robb, J. R. Cheeseman, G. Scalmani, V. Barone, B. Mennucci, G. A. Petersson, H. Nakatsuji, M. Caricato, X. Li, H. P. Hratchian, A. F. Izmaylov, J. Bloino, G. Zheng, J. L. Sonnenberg, M. Hada, M. Ehara, K. Toyota, R. Fukuda, J. Hasegawa, M. Ishida, T. Nakajima, Y. Honda, O. Kitao, H. Nakai, T. Vreven, J. A. Montgomery Jr., J. E. Peralta, F. Ogliaro, M. J. Bearpark, J. J. Heyd, E. Brothers, K. N. Kudin, V. N. Staroverov, R. Kobayashi, J. Normand, K. Rhagavachari, A. Rendell, J. C. Burant, S. S. Iyengar, J. Tomasi, M. Cossi, N. Rega, J. M. Millam, M. Klene, J. E. Knox, J. B. Cross, V. Bakken, C. Adamo, J. Jaramillo, R. Gomperts, R. E. Stratmann, O. Yazyev, A. J. Austin, R. Cammi, C. Pomelli, J. W. Ochterski, R. L. Martin, K. Morokuma, G. Zakrzewski, G. A. Voth, P. Salvador, J. J. Dannenberg, S. Dapprich, A. D. Daniels, O. Farkas, J. B. Foresman, J. V. Ortiz, J. Cioslowski, D. J. Fox, Revision A.02 ed., Gaussian, Inc., Wallingford, CT, **2009**.
[41] a) F. Aquilante, L. De Vico, N. Ferré, G. Ghigo, P.-Å. Malmqvist, P. Neogrady, T. B. Pedersen, M. Pitonak, M. Reiher, B. O. Roos, L. Serrano-Andrés, M. Urban, V. Veryazov, R. Lindh, *J. Comput. Chem.* **2010**, *31*, 224 – 247; b) F. Aquilante, T. B. Pedersen, V. Veryazov, R. Lindh, *WIREs Comput. Mol. Sci.* **2013**, *3*, 143 – 149; c) F. Aquilante, J. Autschbach, R. K. Carlson, L. F. Chibotaru, M. G. Delcey, L. De Vico, I. Fdez Galván, N. Ferré, L. M. Frutos,

L. Gagliardi, M. Garavelli, A. Giussani, C. E. Hoyer, G. Li Manni, H. Lischka, D. Ma, P.-Å. Malmqvist, T. Müller, A. Nenov, M. Olivucci, T. B. Pedersen, D. Peng, F. Plasser, B. Pritchard, M. Reiher, I. Rivalta, I. Schapiro, J. Segarra-Martí, M. Stenrup, D. G. Truhlar, L. Ungur, A. Valentini, S. Vancoillie, V. Veryazov, V. P. Vysotskiy, O. Weingart, F. Zapata, R. Lindh, *J. Comput. Chem.* **2016**, *37*, 506 – 541.

[42] K. Pierloot, B. Dumez, P. O. Widmark, B. O. Roos, *Theor. Chim. Acta* **1995**, *90*, 87 – 114.

[43] A. K. Rappe, W. A. Goddard, *J. Phys. Chem.* **1991**, *95*, 3358 – 3363.

[44] a) D. Abramavicius, B. Palmieri, D. V. Voronine, F. Sanda, S. Mukamel, *Chem. Rev.* **2009**, *109*, 2350 – 2408; b) I. Rivalta, A. Nenov, O. Weingart, G. Cerullo, M. Garavelli, S. Mukamel, *J. Phys. Chem. B* **2014**, *118*, 8396 – 8405.

[45] a) I. Rivalta, A. Nenov, G. Cerullo, S. Mukamel, M. Garavelli, *Int. J. Quantum Chem.* **2014**, *114*, 85 – 93; b) G. H. Chen, S. Mukamel, D. Beljonne, J. L. Bredas, *J. Chem. Phys.* **1996**, *104*, 5406 – 5414.

[46] S. Mukamel, *Principles of Nonlinear Optical Spectroscopy*, Oxford University Press, New York, **1995**.

[47] A. Nenov, A. Giussani, B. P. Fingerhut, I. Rivalta, E. Dumont, S. Mukamel, M. Garavelli, *Phys. Chem. Chem. Phys.* **2015**, *17*, 30925 – 30936.

[48] A. Nenov, J. Segarra-Martí, A. Giussani, I. Conti, I. Rivalta, E. Dumont, V. K. Jaiswal, S. F. Altavilla, S. Mukamel, M. Garavelli, *Faraday Discuss.* **2015**, *177*, 345 – 362.

Received: December 18, 2015
Published online on April 26, 2016

